Validation of Himawari-8 aerosol optical depth retrievals over China

Zhaoyang Zhang[a],[*], Weiling Wu[b], Meng Fan[c], Minghui Tao[d], Jing Wei[e], Jia Jin[a], Yunhui Tan[a], Quan Wang[f],[**]

[a] College of Geography and Environmental Sciences, Zhejiang Normal University, Zhejiang Province, China
[b] Chinese Academy for Environmental Planning, Beijing, China
[c] State Key Laboratory of Remote Sensing Science, Institute of Remote Sensing and Digital Earth, Chinese Academy of Sciences, Beijing, China
[d] School of Earth Sciences, China University of Geosciences, Wuhan, China
[e] State Key Laboratory of Earth Surface Processes and Resource Ecology, College of Global Change and Earth System Science, Beijing Normal University, Beijing, China
[f] Faculty of Agriculture, Shizuoka University, Shizuoka, Japan

ARTICLE INFO

ABSTRACT

High temporal resolution (every 10 min) aerosol observations are rarely provided by satellite sensors. The Advanced Himawari Imager (AHI) aboard Himawari-8 can provide aerosol optical depth (AOD) over China with this frequency. The sensor provides great opportunity to retrieve the particle matter near the ground and improve air quality modeling using the aerosol products. However, there is still lack of quality validation about AHI AOD. A comprehensive research was conducted to evaluate the performance of AHI aerosol products based on sixteen sun-photometers stations in AErosol RObotic NETwork (AERONET) and Sun–Sky Radiometer Observation Network (SONET) over China. The overall comparison of AHI AOD and ground AOD shows a high correlation (R^2 = 0.67). However, there is only 55% of AHI AOD falling in the expected error envelops ($\pm$ 0.05 $\pm$ 0.2*AOD $_{ground}$). AOD bias between AHI AOD and ground AOD increases with the AOD magnitude. The accuracy of AHI AOD is also highly depend on seasons and surface land cover types. Best performance of AHI aerosol retrievals is shown in summer and for urban region. The diurnal variability validation shows that AHI AOD catch the diurnal AOD variations well, especially for summer. Large differences between AHI AOD and MODerate-resolution Imaging Spectrometer (MODIS) aerosol products are shown, especially for northwest China. The analysis indicates that the uncertainties of AHI aerosol retrievals are induced by large errors of aerosol models and surface reflectance estimation in the algorithm.

1. Introduction

Aerosols encompasses a wide range of particles in atmosphere, which have different compositions, sizes, shapes, and optical properties (Hinds, 1999). Atmospheric aerosols have large impacts on human health, environment, and climate change (WHO, 2005; Kodros et al., 2015; Zhang et al., 2017a). A rapidly increase of small aerosol particles less than 2.5 μm near surface in short time can increase the hospital admission (WHO, 2005). The increased aerosol loadings can reduce the visibility and destroy the environment (Zhang et al., 2016a). Aerosols also affect the atmospheric radiative balance (Malm et al., 1994; Kim et al., 2006; Ezhova et al., 2018), and it represents one of the largest uncertainties in climate studies (Field et al., 2014).

Aerosol Optical Depth (AOD) is the fundamental aerosol optical property and can be used to quantify the amount of aerosol particles.

AOD can be retrieved from ground-based sun-photometer and space-borne satellite sensors. Due to the limited number of ground-based stations, it is hard to meet the need for characterizing the variability of regional aerosols in large regions. The launch of satellite sensors provides great opportunities to address this problem. There are many studies conducting to evaluate the accuracies of satellite sensors in the retrieval of AOD. Many researches demonstrated that the retrieval of aerosol from satellites has large improvements (Li et al., 2013; Zhang et al., 2016b). However, there are still many uncertainties in satellite aerosol datasets due to the influence of heavy polluted aerosol layer (Li et al., 2009; Tao et al., 2015) and approximations existed in the aerosol retrievals (Tao et al., 2017). For example, limited aerosol models were used in the aerosol algorithm and this might induce large uncertainties in retrieving AOD (Tao et al., 2017). The simplified radiative equation in some aerosol algorithm also brought some errors because of the

Table 1
Aerosol optical properties adopted in AHI aerosol algorithm (The second row is single scattering albedo (SSA) at 673 nm; The third row is real refractive index (r) at 673 nm; The fourth row is imaginary refractive index (m) at 673 nm).

	Fine mode						Coarse mode	
SSA	0.93	0.8	0.88	0.92	0.93	0.72	0.93	0.93
r	1.452	1.5202	1.4494	1.4098	1.3943	1.4104	1.362	1.452
m	0.0036	0.0245	0.0092	0.0063	0.0044	0.0337	$3*10^{-9}$	0.0036

Table 2
Surface type and location for each ground station.

No.	Station Name	Latitude	Longitude	Altitude(m)	Surface Type
1	AOE_Baotou	40.852	109.629	1270	Grassland
2	Beijing-CAMS	39.933	116.317	106	Urban
3	Beijing	39.977	116.381	92	Urban
4	Beijing_PKU	39.992	116.310	53	Urban
5	Beijing_RADI	40.005	116.379	59	Urban
6	Hong_Kong_PolyU	22.303	114.18	30	Urban
7	QOMS_CAS	28.365	86.948	4276	Grassland
8	SONET_Harbin	45.705	126.614	187	Urban
9	SONET_Hefei	31.905	117.162	36	Cropland
10	SONET_Nanjing	32.115	118.957	52	Urban
11	SONET_Shanghai	31.284	121.481	84	Urban
12	SONET_Xingtai	37.182	114.360	185	Cropland
13	SONET_Zhoushan	29.994	122.188	29	Cropland
14	Taihu	31.421	120.215	20	Wetland
15	Xianghe	39.754	116.962	36	Cropland
16	XuZhou-CUMT	34.217	117.142	59	Cropland

missing of multiple scattering (Yan et al., 2018). Therefore, widely validations based on ground-based sun-photometer are needed to evaluate the performance of satellite aerosol products, especially for the diurnal variability of satellite.

Himawari-8 was launched in October 2014 and carried a new payload called the Advanced Himawari Imager (AHI). This satellite is a geostationary weather satellite and can provide aerosol information every 10 min over East Asia, Southeast Asia, part of South Asia, and Oceania. It is one of the few sensors that can provide diurnal variability of AOD. The algorithm of aerosol retrievals over land used in Himawari-8 was similar to Deep Blue (DB) method (Yoshida et al., 2018). The surface reflectance of visible band is determined as the second lowest reflectance in one month (Kumabe et al., 1996). Due to the advantage of high temporal resolutions, the aerosol products have been used for aerosol data assimilation (Yumimoto et al., 2016). However, to our knowledge, there has been no comprehensive research about the large-scale accuracy of AHI aerosol retrievals.

In recent years, China suffers relatively high aerosol loading compared with nominal global conditions (Boucher et al., 2013). Within this context, it is essential to understand the temporal and spatial characteristic of AOD in China. Himawari-8 is an important instrument to understand the aerosol pollution in China. In this paper, the AHI AOD is firstly validated using ground-based sun-photometers over China. Diurnal variability and regional accuracies of AHI AOD over study region are also evaluated. The objective in this study is to perform a comprehensive validation of AHI AOD retrievals with ground measurements over China to evaluate the performance of AHI aerosol data and to make certain that the products are robust and meet the level of accuracy for aerosol monitoring. This paper is organized as follows: description of data is outlined in Section 2. In Section 3, the comparison of AHI aerosol retrievals against ground data is shown. Section 4 presents the comparison between regional AHI AOD and Moderate

Resolution Imaging Spectroradiometer (MODIS) measurements. Section 5 summaries the main findings.

2. Data

2.1. AHI AOD

The AHI AOD product at 500 nm is retrieved using the pre-calculated surface reflectance database. The surface reflectance database was created using second lowest land surface reflectance in a month over land and calculated sea surface reflectance based on the model developed by Cox and Munk (1954) and observed wind speed from JMA global analysis (GANAL) data (Onogi et al., 2007). Total ozone columns from the Ozone Monitoring Instrument (OMI) on board the NASA EOS/Aura and the column water vapor obtained from GANAL data are conducted for gas correction. The aerosol model in the AHI aerosol retrieval algorithm is made up of external mixture of fine and coarse aerosol particles. Fine aerosol model is based on the average properties of the fine mode for category 1–6 by Omar et al. (2005) (Table 1), which provide the global aerosol models using Aerosol Robotic Network (AERONET) (Holben et al., 1998) measurements. For the coarse aerosol model, the external mixture of the pure marine aerosol on the basis of the model illustrated by Sayer et al. (2012) and a dust model based on the coarse model of category 1 (dust) illustrated by Omar et al.
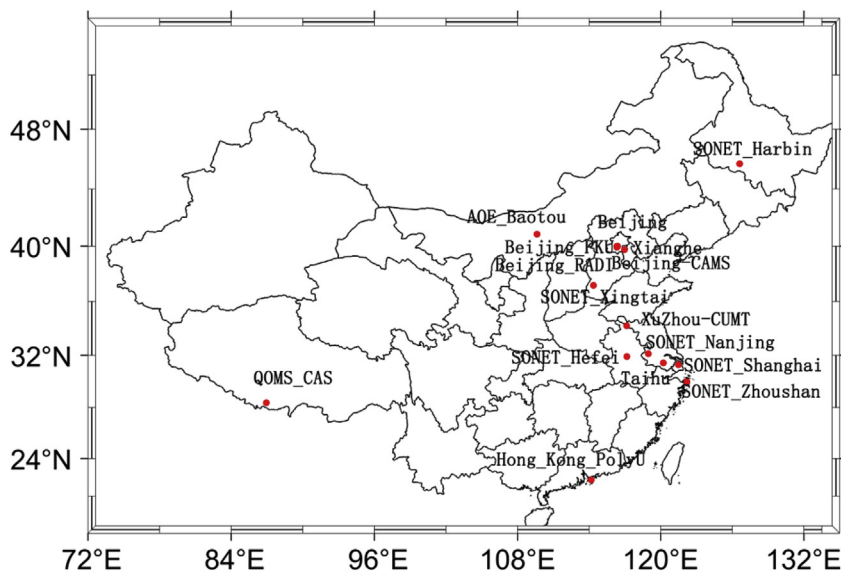

Fig. 1. Map of the selected ground station.

Table 3
Analysis of various spatial and temporal window for AHI AOD.

	Time ≤ 2 min			Time ≤ 5 min			Time ≤ 7 min			Time ≤ 10 min			Time ≤ 20 min		
	Sample size	R^2	RMSE	Sample size	R^2	RMSE	Sample size	R^2	RMSE	Sample size	R^2	RMSE	Sample size	R^2	RMSE
r = 1 pixel	11763	0.63	0.32	19001	0.62	0.32	22170	0.62	0.32	23978	0.61	0.32	26422	0.6	0.32
r ≤ 3 pixels	11859	0.65	0.32	19038	0.64	0.31	22132	0.64	0.31	23928	0.64	0.3	26372	0.64	0.3
r ≤ 6 pixels	11758	0.68	0.3	18768	0.67	0.3	**21749**	**0.67**	**0.3**	23491	0.67	0.3	25975	0.66	0.3
r ≤ 12 pixels	11568	0.65	0.32	18427	0.64	0.31	21247	0.65	0.31	22949	0.64	0.31	25440	0.64	0.31

Fig. 2. Comparison of AHI AOD with ground AOD (EE1 represents the expected error from MODIS DB products (black dot line) and EE2 is the EE from GCOS; blue line is the 1:1 line; pink circles are the mean AOD for AOD bins and pink lines are standard deviation). (For interpretation of the references to color in this figure legend, the reader is referred to the Web version of this article.)

(2005) is adopted in the algorithm. Detailed information about the aerosol retrieval algorithm can be found in Yoshida et al. (2018). Level 2 and Level 3 AHI aerosol datasets are two kinds of products in Himawari-8 with the same spatial resolution of 5 km (Kikuchi et al., 2018). The temporal resolution of Level 2 and Level 3 products is 10 min and 1 h, respectively. Level 2 version 2 aerosol datasets from January 2016 to December 2016 are used in this study. Due to the

location of sun-photometer, we only validate the AOD over land.

2.2. MODIS AOD

MODIS AOD is the most common used AOD data and are applied in many fields (Tao et al., 2013; Wang et al., 2014; Tie et al., 2016; Zhang et al., 2017b; Zhang and Wong, 2017). MODIS Collection 6.1 products from the Aqua satellite during January 2016 to December 2016 are used to evaluate the regional distribution of AHI AOD. AOD over land in MODIS is retrieved using two different algorithms: Dark-Target (DT) (Levy et al., 2010) and Deep-Blue (DB) (Hsu et al., 2004, 2013) algorithms. The expected errors of DT and DB AOD over land are within $\pm\ 0.05\ \pm\ 0.15 \times AOD_{AERONET}$ (Levy et al., 2013) and $\pm\ 0.05\ \pm\ 0.2 \times AOD_{AERONET}$ (Sayer et al., 2013), respectively. The DB Expected error (EE1) is used to compare the performance of AHI AOD with MODIS AOD retrievals. Global climate observation system (GCOS) goal uncertainty (Max (0.03; 10%), EE2) is also used as a metric (GCOS, 2006). DB and DT combined land product is used in this paper. The resolution of aerosol datasets (MYD04) in MODIS is 10 km. To compare this product with AHI AOD, both aerosol products are resampled in the resolution of 1°. The MODIS retrievals are assigned to the AHI pixel location nearest the MODIS retrieval center. The MODIS DT and DB combined AOD are converted from 550 nm to 500 nm.

2.3. AERONET AOD

To reconcile satellite-based dataset, ground-based AOD measurements collected from sun-photometer in the AERONET (Holben et al., 1998) and Sun–Sky Radiometer Observation Network (SONET) (Li et al., 2018) are considered. In this paper, 16 selected ground stations are mapped in Fig. 1. AERONET AOD data have higher accuracy of <
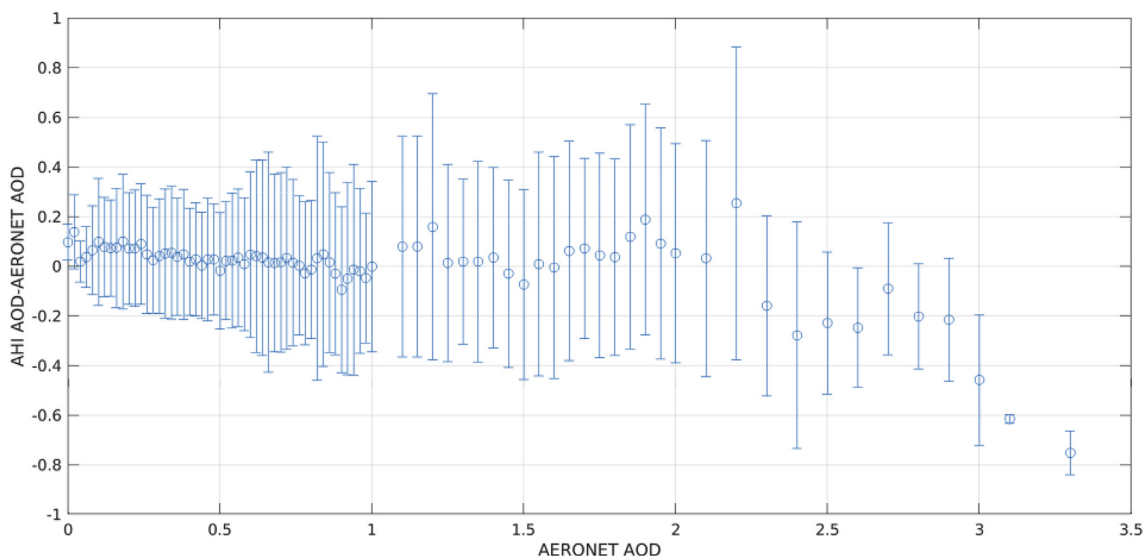

Fig. 3. The bias between AHI AOD and ground AOD versus ground AOD with mean (blue circle) and standard deviation (blue line). (For interpretation of the references to color in this figure legend, the reader is referred to the Web version of this article.)
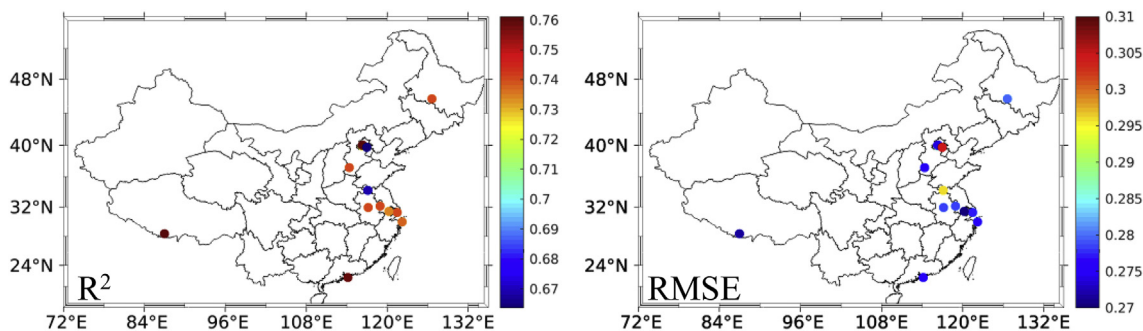
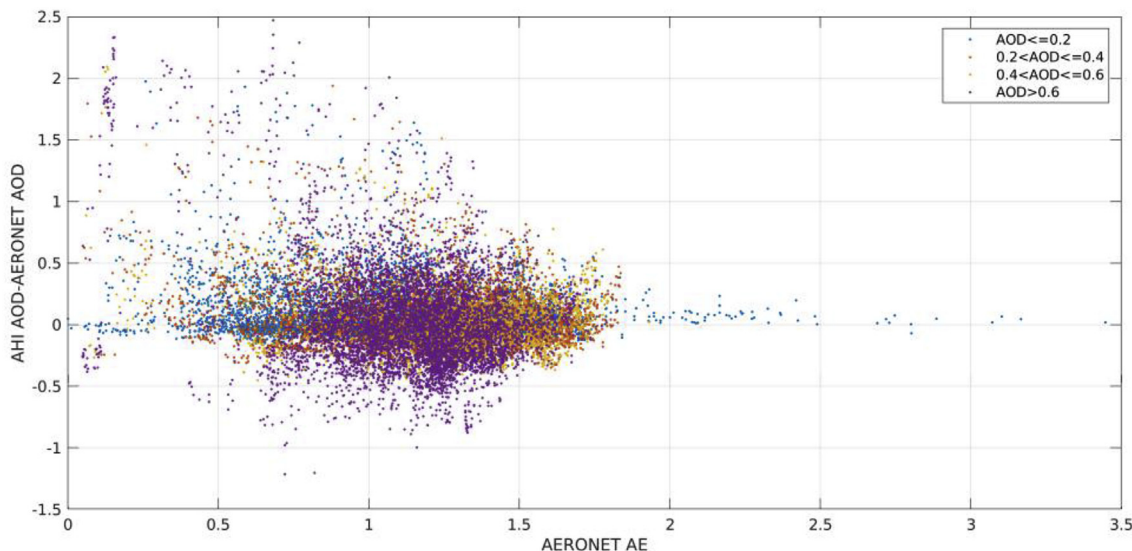**Fig. 4.** The spatial distribution of R^2 and RMSE between AHI AOD and ground AOD.

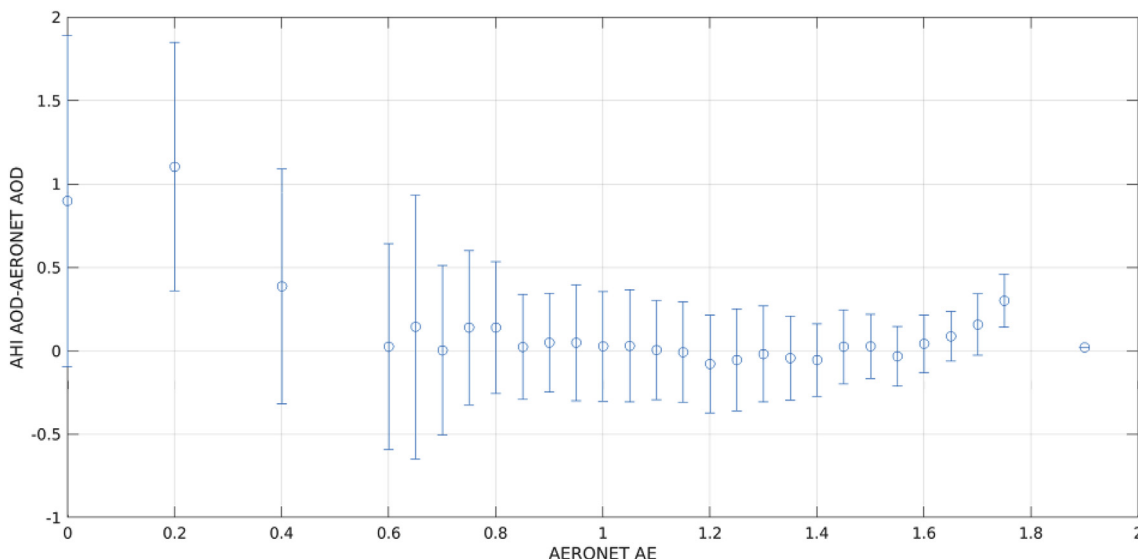**Fig. 5.** The bias between AHI AOD and ground AOD versus ground Ångström exponent.

Fig. 6. The bias between AHI AOD and ground AOD versus ground Ångström Exponent for ground AOD > 0.4 with mean (blue circle) and standard deviation (blue line). (For interpretation of the references to color in this figure legend, the reader is referred to the Web version of this article.)

± 0.01 for retrieval at wavelengths longer than 440 nm and < ± 0.02 for shorter wavelengths without cloud contamination (Holben et al., 1998). AERONET AOD bias can reach at 0.031–0.060 due to thin cirrus cloud contamination (Chew et al., 2011). These data become an important regional context to ensure representativeness of the satellite data. In order to evaluate the accuracy of AHI AOD, AERONET and SONET level 2 version 3 AOD data were used in this paper. Level 1.5 AOD datasets are used if it is not yet available for particular site. The SONET is a ground-based Cimel radiometer network with the extension of multiwavelength polarization measurement capability to observe
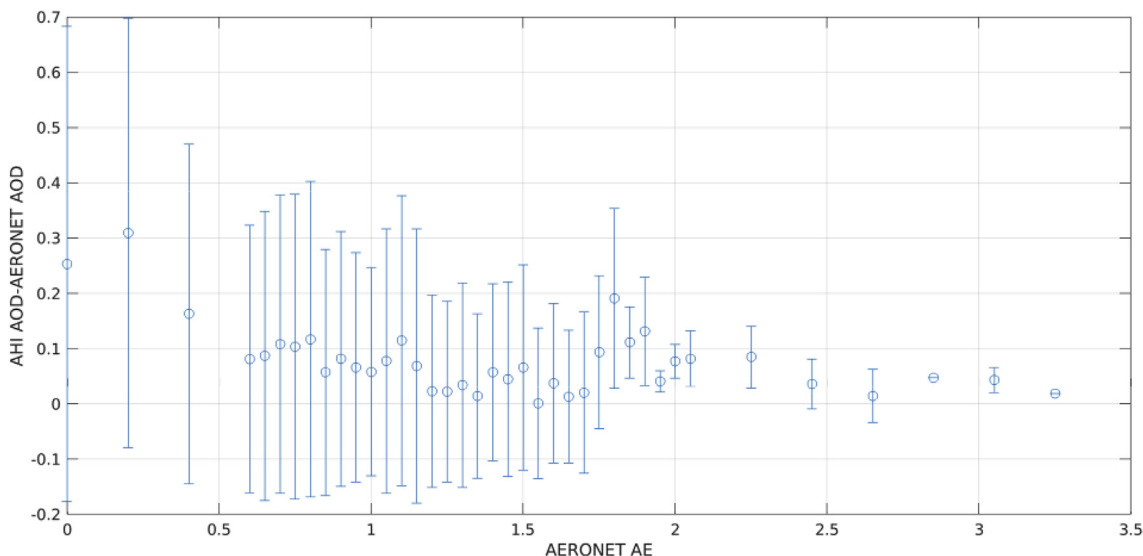
Fig. 7. The bias between AHI AOD and ground AOD versus ground Ångström Exponent for ground AOD ≤ 0.4 with mean (blue circle) and standard deviation (blue line). (For interpretation of the references to color in this figure legend, the reader is referred to the Web version of this article.)
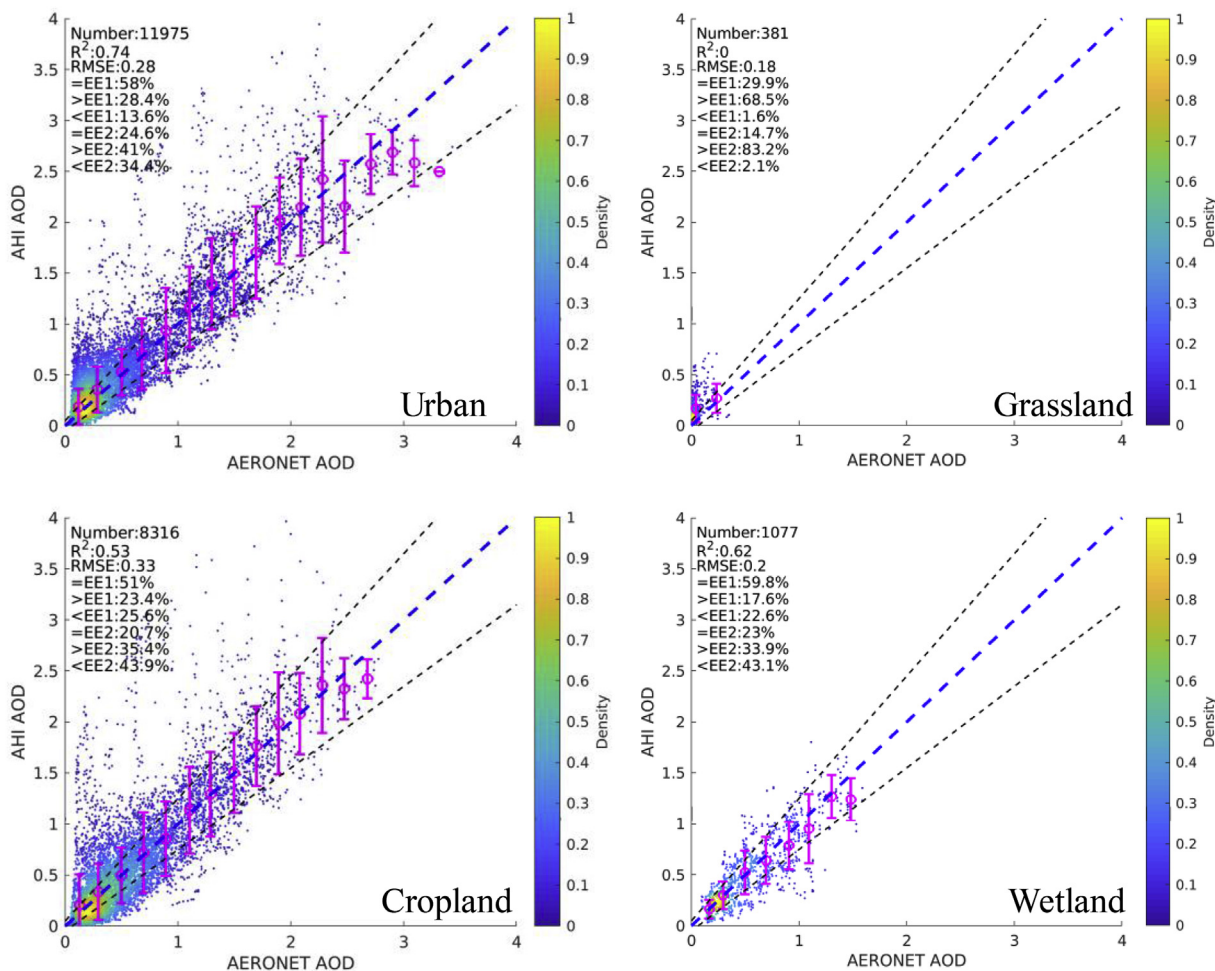

Fig. 8. Scatter plots of AHI AOD and ground AOD for different land cover (EE1 represents the expected error from MODIS DB products (black dot line) and EE2 is the EE from GCOS; blue line is the 1:1 line; pink circles are the mean AOD for AOD bins and pink lines are standard deviation). (For interpretation of the references to color in this figure legend, the reader is referred to the Web version of this article.)

long-term columnar atmospheric aerosol properties over China (Li et al., 2018). For sun-photometer in ground stations does not have 500 nm channel, the AOD in 500 nm is calculated using Ångström exponent and AOD in 675 nm and 440 nm (Tao et al., 2015). Table 2 shows the specific locations and land cover of each ground station in mainland of China (Wei et al., 2018).
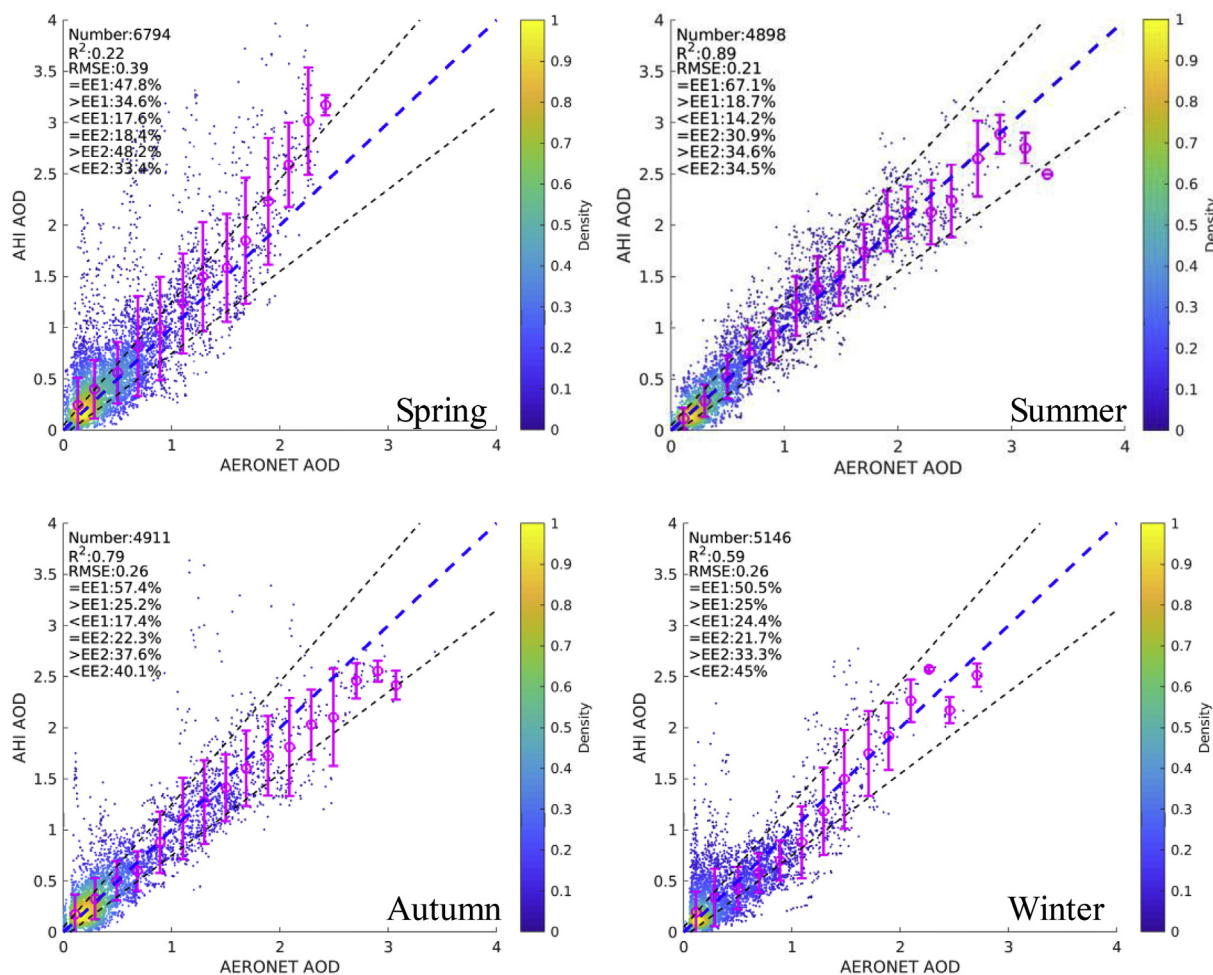
Fig. 9. Scatter plots of AHI AOD and ground AOD for different seasons (a. spring, b. summer, c. autumn, d. winter) (EE1 represents the expected error from MODIS DB products (black dot line) and EE2 is the EE from GCOS; blue line is the 1:1 line; pink circles are the mean AOD for AOD bins and pink lines are standard deviation). (For interpretation of the references to color in this figure legend, the reader is referred to the Web version of this article.)

Table 4
Analysis of AHI AOD and ground AOD in different land cover at autumn, spring, summer, and winter.

Land Cover	Seasons	Sample size	R^2	RMSE	Within EE1 (%)	> EE1 (%)	< EE1 (%)
urban	Autumn	3020	0.82	0.25	61.1	24.1	14.8
	Spring	3218	0.24	0.39	46.6	40.6	12.8
	Summer	1477	0.84	0.22	60.5	18.4	21.1
	Winter	2077	0.53	0.3	46	17.1	36.9
grassland	Autumn	149	0	0.123	48.9	48.3	2.8
	Spring	181	0	0.22	27.1	71.3	1.7
	Summer	40	0	0.19	20	72.5	7.5
	Winter	11	0	0.05	81.8	18.2	0
cropland	Autumn	1742	0.72	0.29	53.1	23.5	23.4
	Spring	3020	0.09	0.41	48.7	29.9	21.4
	Summer	1477	0.84	0.22	60.5	18.4	21.1
	Winter	2077	0.53	0.3	46	17.1	36.9
wetland	Autumn	/	/	/	/	/	/
	Spring	375	0.59	0.24	60.5	2.9	36.5
	Summer	421	0.69	0.18	64.6	34.9	0.5
	Winter	281	0.49	0.18	51.6	11.4	37

2.4. Spatiotemporal window

New-generation geostationary meteorological satellite sensors provide data with large spatial coverage and high temporal resolution (10 min), while the ground-based observations provide high temporal site data (15 min). AOD retrievals within same time intervals and spatial windows are used for validation because of the relative homogeneous aerosol properties within a certain time-space boundary (Anderson et al., 2003). In this paper, five-time intervals from 2 to 20 min centered at satellite overpass time and four spatial windows from 1 pixel to 12 pixels centered at each site point were used. The selected spatial and temporal window are committed to a better balance between sample size and correlation quality (Martins et al., 2017). Table 3 shows the results with different spatial and temporal windows
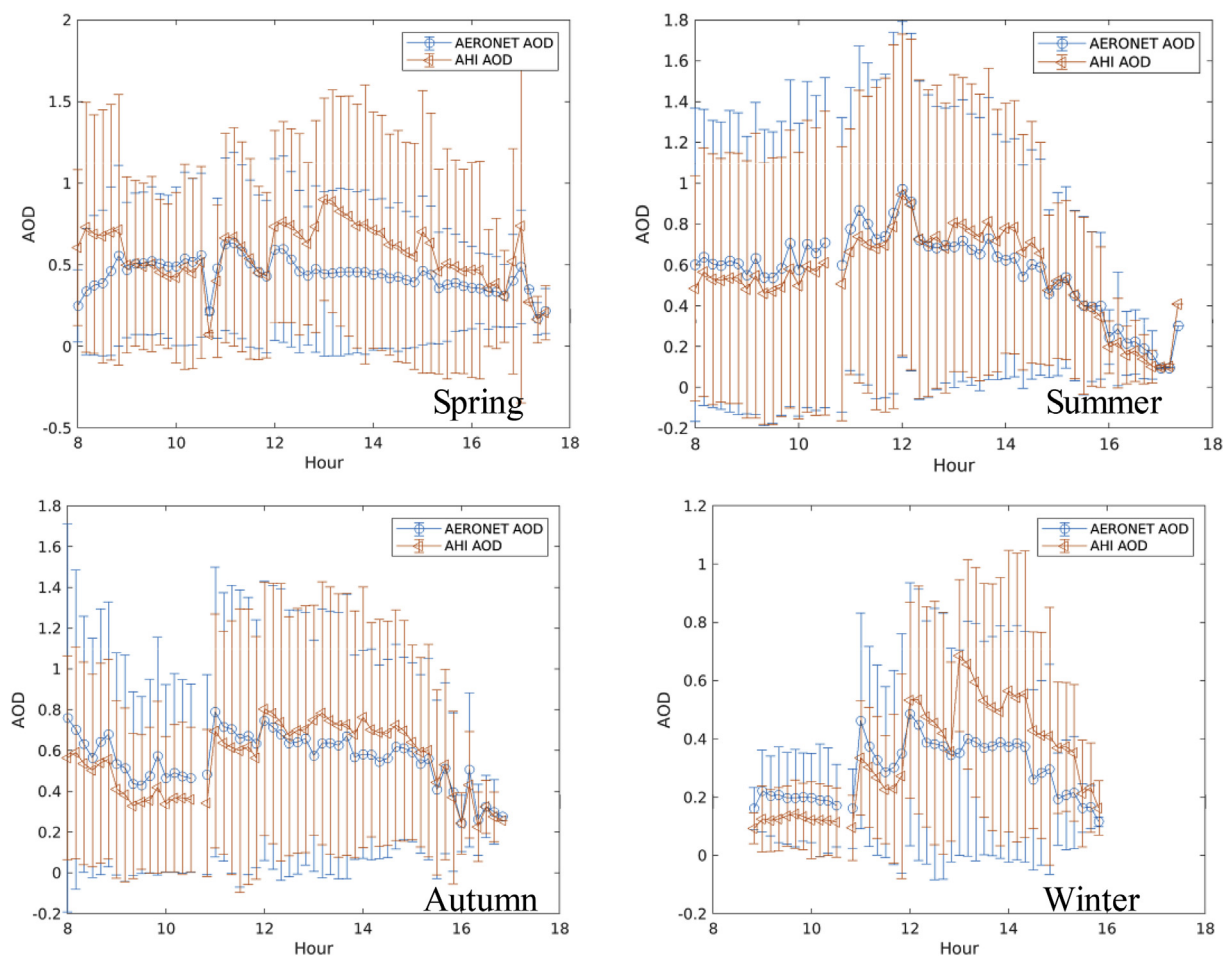
Fig. 10. Diurnal variations (8:00–18:00 local time) of AHI AOD and ground AOD in different seasons with mean (blue circle and orange triangle) and standard deviation (blue and orange line) for urban. (For interpretation of the references to color in this figure legend, the reader is referred to the Web version of this article.)

for AHI AOD. Highest correlation and smallest Root Mean Square Error (RMSE) are expected with minimum time lag and smallest window size. However, the analysis from Table 3 indicates that correlation decreases with temporal window and sample size increases with temporal window. The average AOD is adopted if more than 40% validated values are in the sample size (Martins et al., 2017). Highest correlation ($R^2 = 0.67$) occurs at the window of radius ≤ 6 pixels and time ≤ 7 min with an RMSE of 0.3. For the window with same radius, the sample size increases from 11763 (time ≤ 2 min) to 19001 (time ≤ 5 min) with a little change in correlation. To increase the sample size, we select the window of r ≤ 6 pixels and time ≤ 7 min as the balanced window. The comparisons of AHI AOD and ground AOD are based on the large windows to balance the measurements size and correlation quality. Previous validation of satellite sensors also employs the relatively large spatial regions and time intervals to comprise the balance of measurements size and correlation quality (Levy et al., 2010; Tao et al., 2015).

3. Results and discussion

3.1. Overall AHI and ground AOD comparison

Fig. 2 shows the scatter plots of AHI AOD against ground AOD. Blue line represents one-to-one line and black lines are the envelope of expected error. The sample size is about 21749 with R^2 of 0.67. There are about 55% of AOD values within the envelopes of expected error, 26.6% of them are larger than expected errors, and 18.4% are smaller than the expected error lines. For MODIS products, there are more than

69.25% of DT retrievals falling in the expected error envelops ($\pm 0.05 \pm 0.15 \times$ AOD) over China (Wei et al., 2018). According to the EE2 from GCOS, only 22.9% of AOD retrievals fall within the metric. The results indicate that the AHI overestimates the aerosol loadings. Most AOD values are from 0 to 1. According to the standard deviation in AOD bins, the standard deviation increased with AOD when AOD is lower than ∼2.5. Fig. 3 shows the bias between AHI AOD and ground AOD versus ground AOD. The bias decreases with the AOD magnitude. Positive bias is shown when the AOD is lower than 0.5. The bias can reach at −0.8 when the AOD is higher than 3. The analysis indicates that the aerosol model between heavy polluted weather and clear days varies a lot. It is essential to distinguish the correct aerosol model for aerosol retrieval. Fig. 4 shows the spatial distribution of R^2 and RMSE between AHI AOD and ground AOD. The R^2 for all stations are larger than 0.67 and the highest R^2 and lowest R^2 are both shown in Beijing. The RMSE is from ∼0.27 to ∼0.31. The largest RMSE can be found in Beijing.

Ångström exponent (AE) is one indicator of aerosol size, which is calculated by the AOD at 440 nm and 675 nm. AE can help to understand the influence of aerosol size on AOD retrievals. Fig. 5 shows the bias between AHI AOD and ground AOD versus ground Ångström exponent. The bias between AHI AOD and ground AOD versus ground Ångström Exponent for ground AOD > 0.4 and AOD ≤ 0.4 are displayed in Fig. 6 and Fig. 7, respectively. For larger AOD (AOD > 0.4), systemic positive bias is shown. The bias is larger than 0.3 when the AE is smaller than 0.4. Then, the bias was around 0 when the AE is larger than 0.6. For smaller AOD (AOD ≤ 0.4), the bias is relatively small compared with the high AOD group. However, the positive bias is
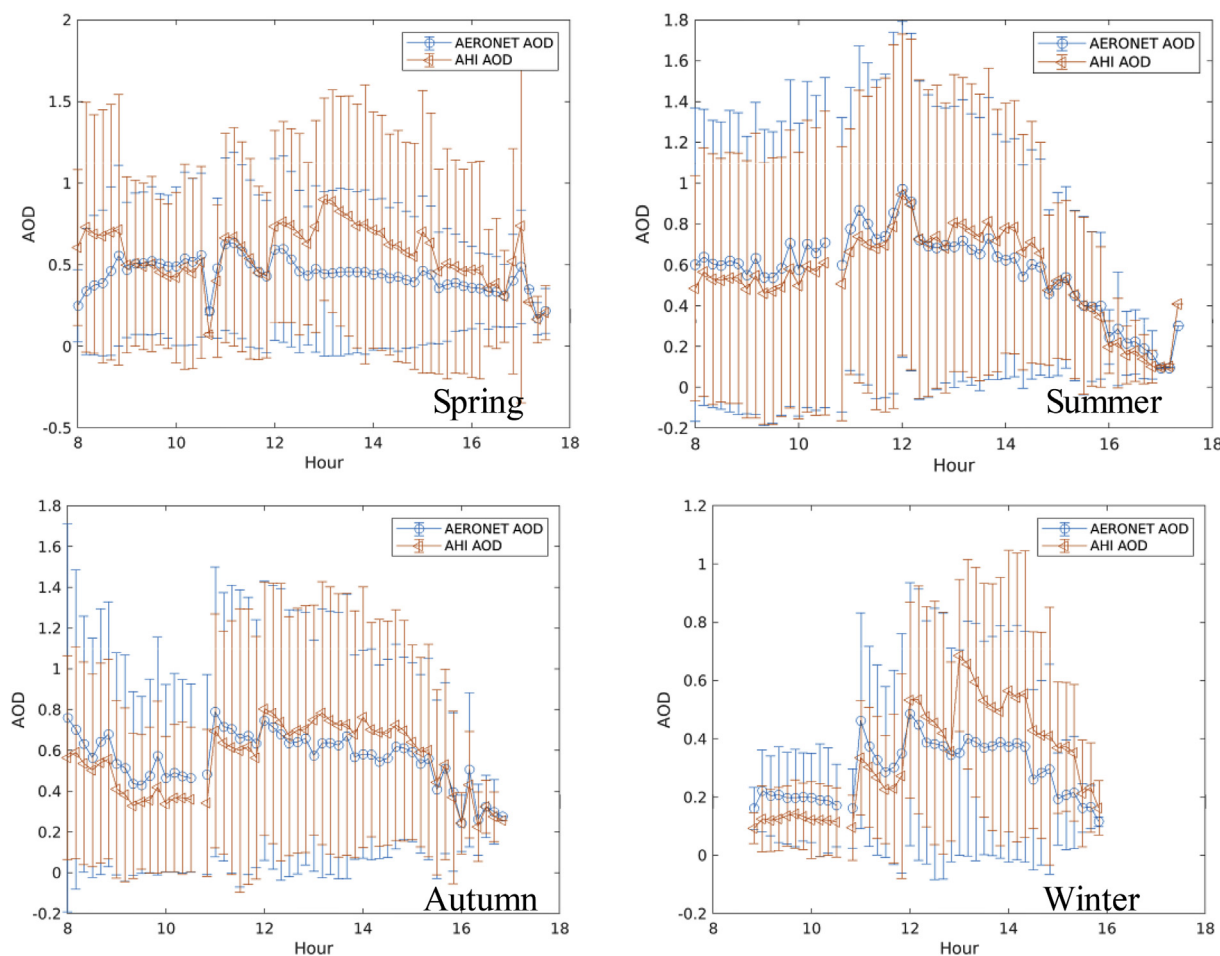
Fig. 11. Same as Fig. 10, but for cropland.

shown. Larger positive bias is shown when AE is smaller than 0.5. The analysis shows that the AHI fails to capture the aerosol model when the aerosol size is very small and the heavy aerosol loadings occurs.

3.2. Comparison of AHI aerosol retrieval against ground data over land cover types

Surface reflectance is one of the important factors that could affect the accuracy of aerosol retrievals significantly. Different land types have different characteristics. Cropland and grassland show large seasonal variations, while urban land has little seasonal changes with obvious surface bidirectional reflectance characteristic (Xie et al., 2017). AHI aerosol algorithm assumes that surface reflectance has little changes in 30 days. The assumption is like the DB aerosol algorithm and could affect the accuracy of AHI AOD. Fig. 8 shows the scatter plots of AHI AOD and ground AOD in urban, cropland, grassland, and wetland regions. Best performance can be found in urban ground stations, with R^2 of 0.74 and RMSE of 0.28. The R^2 in cropland is about 0.53, with 51.3% falling in EE1 envelop and 20.7% falling in EE2 envelop. In wetland, The R^2 and RMSE are 0.62 and 0.2, respectively. Pixels in grassland exhibit poor performance in aerosol retrievals. This might be induced by the low number of retrievals and the AHI aerosol retrievals is very poor when the AOD is low. The analysis indicates that the AHI aerosol retrievals are efficient for urban and wetland regions, and the accuracy of surface reflectance database over grassland and cropland is needed to improve.

3.3. Impacts of seasonal variability on AOD retrievals

China suffers different aerosol types in spring (March, April, May), summer (June, July, August), autumn (September, October, November), and winter (December, January, February). In spring, dust aerosols influence China significantly, especially for North China (Zhang et al., 2016b). Biomass burning aerosols affect China a lot in summer (Long et al., 2016). In winter, the stable weather could induce the accumulation of aerosol and form severe polluted days (Zhang et al., 2018). The changes of surface reflectance in different seasons could also affect the performance of aerosol retrievals (Mhawish et al., 2017). Therefore, it is essential to evaluate the effect of seasonal variations of surface reflectance and aerosol models on AHI retrievals. Seasonal comparisons of AHI AOD and ground AOD are shown in Fig. 9. The R^2 is 0.22, 0.89, 0.79, and 0.59 in spring, summer, autumn, and winter respectively. There are more than 57% of AHI AOD retrievals within the expected error envelops in summer and autumn. In winter, there are also more than 50% of AOD falling in the envelops of EE. In spring, only 47.8% of AHI AOD within the expected error lines and about 34.6% of AHI AOD are larger than the expected error envelops. For the metric from GCOS, less than 31% of the AOD retrievals fall in the EE2. This indicates that the AHI AOD is not accurate enough to be used in climate studies. The result shows that the aerosol retrieval algorithm performs best in summer and performs worst in spring. AHI AOD tends to overestimate the aerosol loadings, especially for spring.

Seasonal analysis for different surface types is conducted to evaluate the temporal performance of AHI aerosol retrieval algorithm. Table 4 show the seasonal performance of AHI aerosol retrievals over different land cover types. In urban, better performance of AHI AOD is shown in
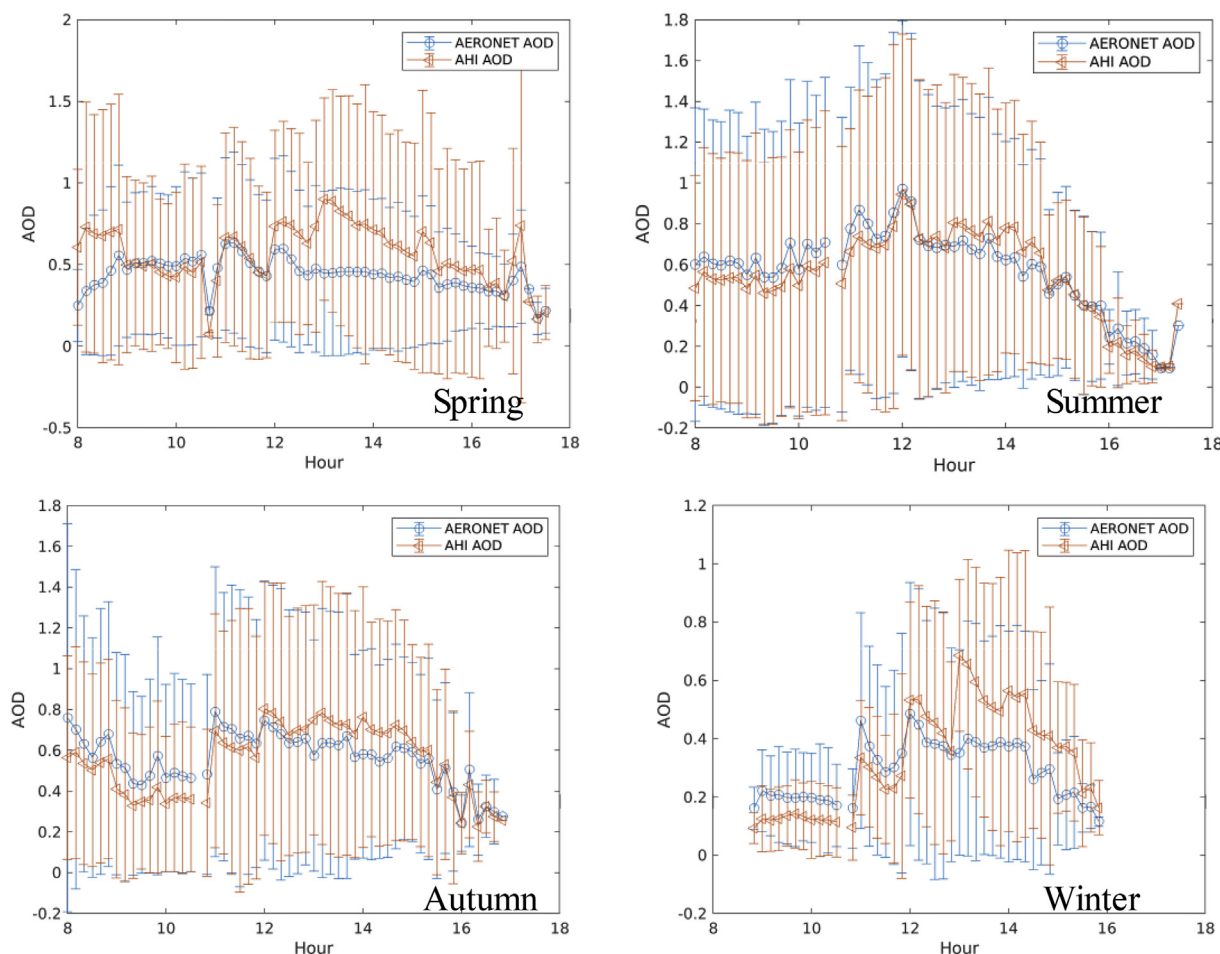
Fig. 12. Same as Fig. 10, but for wetland.

autumn and summer than that in spring and summer. The R^2 is larger than 0.8. There are more than 60% of AHI AOD within the expected error envelops in these two seasons. In grassland, the number of AHI retrievals is very small and AHI aerosol algorithm performs very poor, with R^2 of 0. In cropland, high correlation of AHI AOD and ground AOD occurs in autumn (0.72) and summer (0.84). In wetland, there is no observations in autumn. AHI AOD performs better in summer than in other three seasons. The analysis indicates that the AHI aerosol retrievals are influenced by the seasonal variation of surface reflectance and aerosol models significantly. The AHI aerosol algorithm performs better in summer and autumn than those in other two seasons, except for grassland. Wei et al. (2018) also found similar results that the VIIRS AOD performs better in summer, spring, and autumn.

3.4. Diurnal variability validation

AHI AOD can observe the aerosol information every 10 min in the daytime. Sun photometers in ground stations can measure the AOD every 15 min. Both of these two sensors can reflect the diurnal variability of AOD. Fig. 10 displays the temporal variations of AOD observed by AHI and ground. In urban, the AHI AOD retrievals are higher than the ground observations from 8:00 to ~9:00 in local time and AOD change little from 9:00 to 11:00 (Fig. 10). AOD peak at 13:00 and decrease after 13:00 in spring. In summer, the aerosol loadings increase from 8:00 and peak at 12:00. After 12:00, AOD decrease and reach to the minimum at ~17:00. In summer, the AHI AOD retrievals agree very well with ground measurements and can reflect the diurnal variability of AOD. In winter, highest AOD can be found in the noon (12:00 in local time) from ground-based measurements. However, the AHI AOD peaks

at 13:00. Similar situation can be found in spring. In autumn, high AOD can be found in the morning (8:00 in local time) and AHI underestimates the AOD during this period.

In cropland, similar diurnal variability as in urban is shown in spring and summer (Fig. 11). In autumn, the AOD increase between 8:00 and 12:00 and decrease to minimum at ~16:00. In winter, the AHI AOD increase from ~9:00 to ~15:00. Ground observations show a different trend. The AOD increase from ~9:00 to ~11:00 and decrease to 0.3. In winter, the AOD change little from ~9:00 to ~11:00 and the AOD peak from AHI retrievals and ground measurements is different. Fig. 12 shows the diurnal variability of AOD from AHI and ground in wetland. The decreasing AOD trend can be found in spring and AHI AOD is lower than ground AOD in the morning. The discrepancies between AHI AOD and ground AOD is narrowed from morning to afternoon. There are no observations in autumn. The analysis in this paper shows that the AHI AOD can reflect the diurnal variability well in summer over urban and cropland. For other three seasons, there are some discrepancies between AHI aerosol retrievals and ground-based measurements.

3.5. Comparison between AHI AOD and MODIS datasets

Fig. 13 shows the mean AOD from Himawari and Aqua, and their differences in four seasons. Seasonal comparisons of Himawari AOD with Aqua AOD illustrate that the Himawari overestimated AOD in North China Plain, Northwest China, where have high aerosol loadings. In Spring, high aerosol loadings can be found over East China and West China from Aqua. Although AHI AOD showed some regions with relatively high AOD, the aerosol loadings were significantly overestimated.
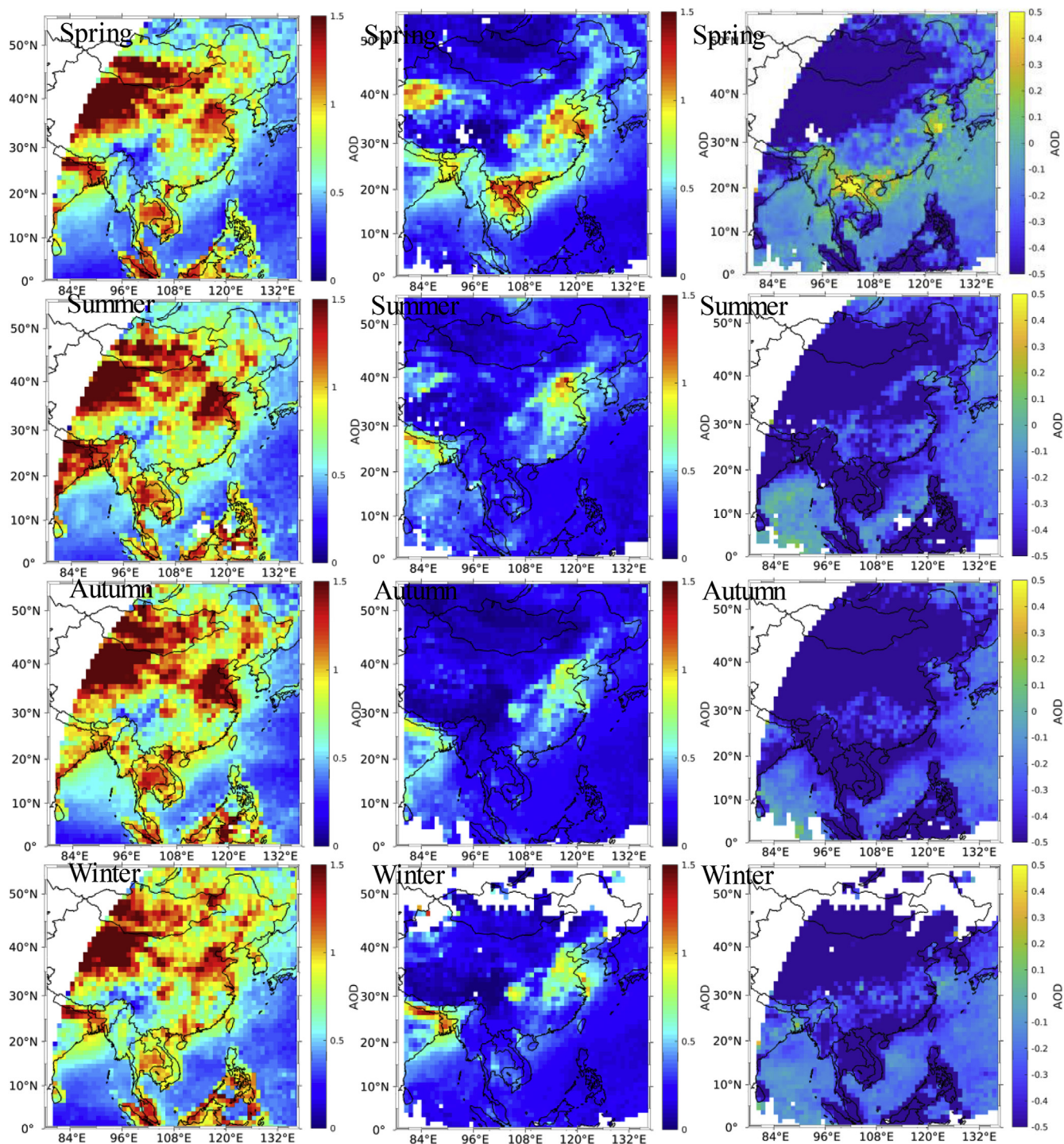
Fig. 13. Mean value of AHI AOD (left), Aqua DB and DT combined AOD (middle), and their difference in spring (March-April-May), summer (June-July-August), autumn (September-October-November), and winter (December-January-February).

The difference between AHI AOD and Aqua AOD can even exceed 0.5 in Northwest China. In summer, large differences were also found in North China Plain. In Autumn, Himawari can reflect the AOD in Southeast China well. However, the AOD in east China is still overestimated. In all, AHI AOD have large uncertainties over land, especially for those regions with high aerosol loadings. The large AOD bias in heavy polluted region could be induced by the large uncertainties of estimation of surface reflectance and aerosol model. Tao et al. (2017) found the change of single scattering albedo leaded large AOD bias. Therefore, it is essential to consider the aerosol optical properties in heavy polluted

weather and create the surface reflectance database based on multi-year satellite data.

Clear days are selected to compare the MODIS DB and DT combined AOD with AHI AOD in Fig. 14. AOD was underestimated by AHI retrievals over North China Plain and lots of pixels were missing. However, MODIS true color image showed no cloud pixels. This might be induced by the optimal estimation method in the aerosol retrieve algorithm. The surface reflectance database in AHI aerosol retrievals is based on finding the second lowest reflectance in one month, which might contain low aerosol information. This causes a bias when low-
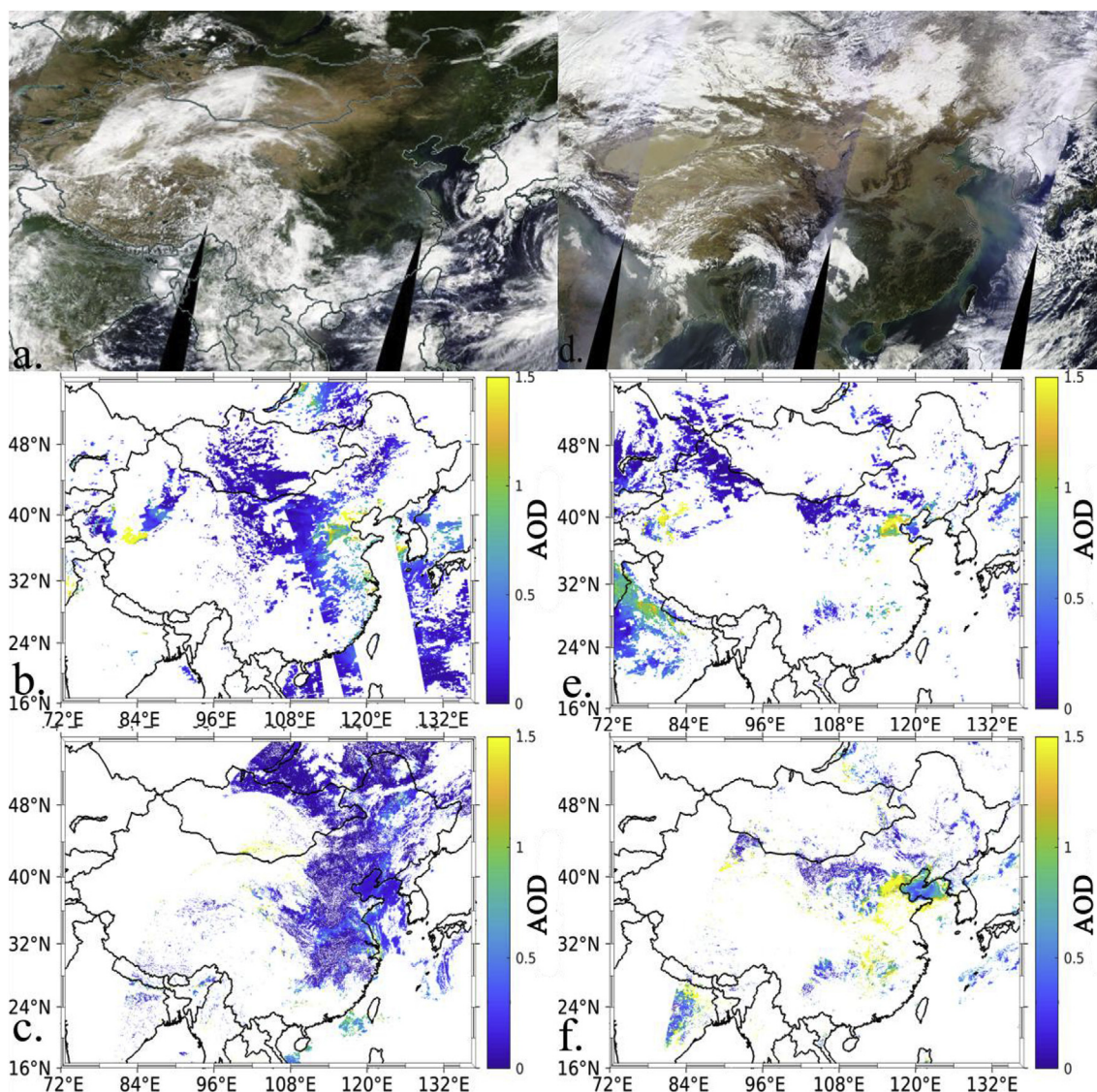
Fig. 14. MODIS true color image (top), MODIS DB and DT combined (middle) and AHI AOD (bottom) on 8 August (a, b, c) and 8 June (e, d, f) 2016. (For interpretation of the references to color in this figure legend, the reader is referred to the Web version of this article.)

AOD conditions are sometimes not retrieved.

Heavy aerosol layer was one of factors that influenced the accuracy of aerosol retrieval. Li et al. (2009) found that the heavy aerosol layer in China could be misclassified as cloud. The MODIS aerosol products improve a lot in retrieving high AOD (Tao et al., 2015). This could also occur in AHI AOD retrievals. Therefore, two haze days were used to compare the AHI AOD with MODIS AOD. According to MODIS true color image, there was no cloud over North China Plain on 5 February 2016. Both AHI AOD and MODIS aerosol retrievals can observe the high aerosol loadings in east China. However, the AHI AOD is very high in northwest China while low AOD can be found from MODIS (Fig. 15). This could be induced by the error of aerosol models in AHI aerosol algorithm. The high AOD in China from MODIS occurs in Jiangsu province and high AOD from AHI measurements shows in Shandong province. This indicates that there are still lots of spaces to improve the AHI aerosol retrievals.

4. Conclusion

Himawari satellite is the new generation geostationary satellite that can be used to retrieve the high temporal resolution of Aerosol Optical Depth (AOD). In this study, we presented a comprehensive research on

evaluating the performance of AOD over China based on sixteen ground-based sun-photometers in AErosol RObotic NETwork (AERONET) and Sun–Sky Radiometer Observation Network (SONET) stations and MODerate-resolution Imaging Spectrometer (MODIS). The R^2 of overall comparison of AHI AOD and ground AOD is 0.67, with about 55% of AHI AOD falling in the envelop of expected error. The bias between AHI AOD and ground AOD is also related with the AOD magnitude. High AOD (> 2.3) is underestimated. Aerosol models also affect the performance of AHI aerosol retrievals. High positive AOD bias are shown when AE is smaller than 0.5. The performance of AHI aerosol algorithm is evaluated as a function of surface types. AHI aerosol retrievals are more efficient for urban ($R^2 = 0.74$) and wetland ($R^2 = 0.62$) than other regions. For different surface types, seasonal changes also influence the performance of aerosol retrievals. Best performance of AHI AOD can be found in summer. Through the diurnal variability validation, decreasing trend of AOD occurs in the afternoon in summer, autumn, and winter. The AHI AOD can reflect the diurnal variability of AOD well in summer. Comparisons of AHI AOD with MODIS regional AOD also indicates that the spatial distribution of AOD from AHI is not very accurate. Clear days show low aerosol conditions are missed due to the uncertainties of aerosol models in the algorithm and larger errors are shown in northwest China. The surface estimation
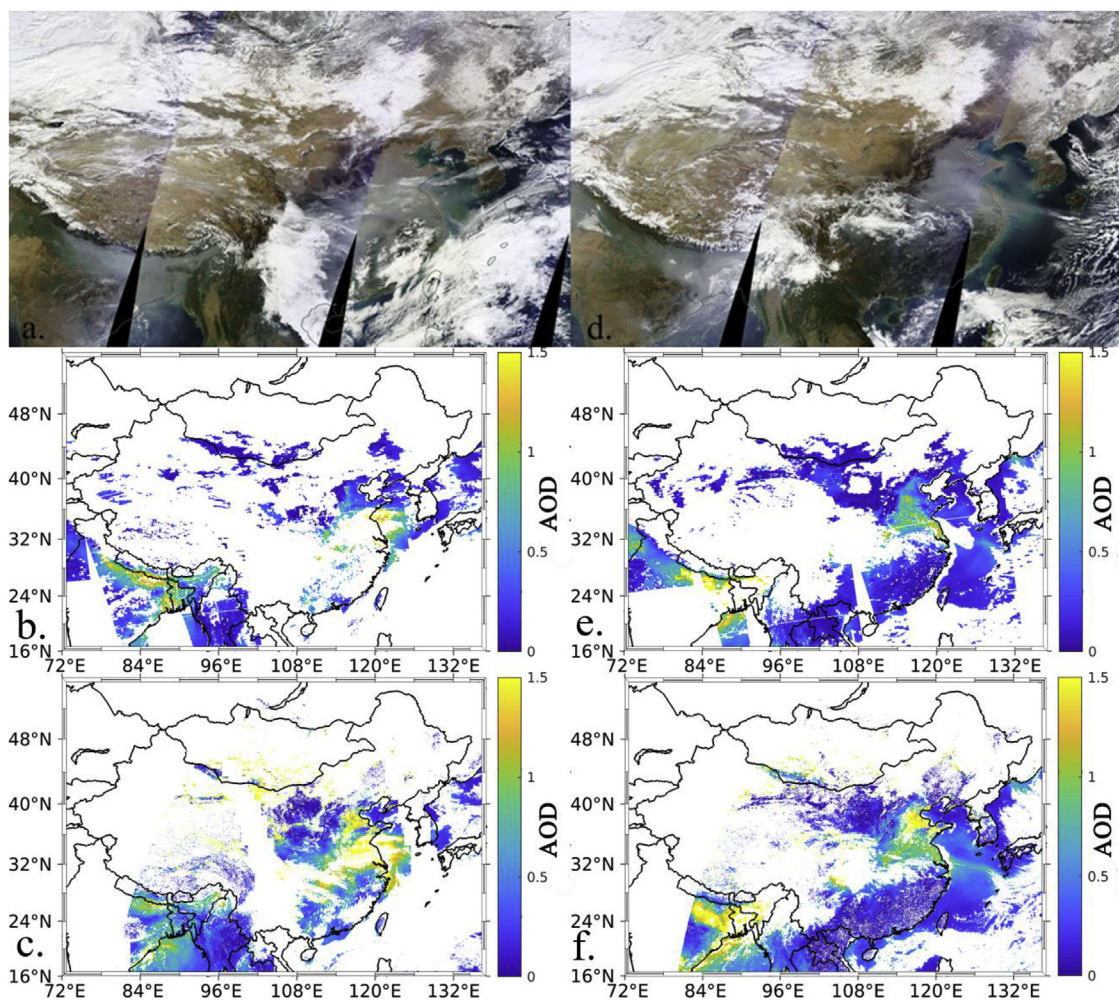
Fig. 15. MODIS true color image (top), MODIS DB and DT combined (middle) and AHI AOD (bottom) on 5 February (a, b, c) and 9 February (e, d, f) 2016. (For interpretation of the references to color in this figure legend, the reader is referred to the Web version of this article.)

and identification of aerosol models in the AHI aerosol algorithm are needed to improve. The analysis in this study investigated the performance of AHI aerosol retrieval algorithm and provided several aspects that can be used to improve the accuracy of AHI AOD.

Appendix A. Supplementary data

Supplementary data to this article can be found online at https://doi.org/10.1016/j.atmosenv.2018.11.024.

References

Anderson, T.L., Charlson, R.J., Winker, D.M., Ogren, J.A., Holmén, K., 2003. Mesoscale variations of tropospheric aerosols. J. Atmos. Sci. 60, 119–136.

Boucher, O., Randall, A.D., Bretherton, P., Feingold, C., Forster, G., Kerminen, P., Kondo, V., Liao, Y., Lohmann, H., Rasch, U., 2013. Clouds and Aerosols in Climate Change 2013, the Physical Science Basis. Contribution of Working Group I to the Fifth Assessment Report of the Intergovernmental Panel on Climate Change. Cambridge University Press Cambridge, United Kingdom and New York, NY, USA.

Chew, B.N., Campbell, J.R., Reid, J.S., Giles, D.M., Welton, E.J., Salinas, S.V., Liew, S.C., 2011. Tropical cirrus cloud contamination in sun photometer data. Atmos. Environ. 45, 6724–6731.

Cox, C.S., Munk, W.H., 1954. Statistics of the sea surface derived from sun glitter. J. Mar. Res. 13, 198–227.

Ezhova, E., Ylivinkka, I., Kuusk, J., Komsaare, K., Vana, M., Krasnova, A., Noe, S., Arshinov, M., Belan, B., Park, S.B., Lavric, J.V., Heimann, M., Petäjä, T., Vesala, T., Mammarella, I., Kolari, P., Bäck, J., Rannik, U., Kerminen, V.M., Kulmala, M., 2018. Direct effect of aerosols on solar radiation and gross primary production in boreal and hemiboreal forests. Atmos. Chem. Phys. Discuss. 2018, 1–27.

Field, C.B., Barros, V.R., Mach, K., Mastrandrea, M., 2014. Climate Change 2014: Impacts, Adaptation, and Vulnerability. Working Group II Contribution to the IPCC 5th Assessment Report-technical Summary. pp. 1–76.

GCOS, 2006. Systematic Observation Requirements for Satellite-based Products for Climate: Supplemental Details to the Satellite-based Component of the "Implementation Plan for the Global Observing System for Climate in Support of the UNFCCC,".

Hinds, W.C., 1999. Aerosol Technology: Properties. Behavior, and Measurement of Airborne Particles. 2nd.

Holben, B.N., Eck, T.F., Slutsker, I., Tanre, D., Buis, J.P., Setzer, A., Vermote, E., Reagan, J.A., Kaufman, Y.J., Nakajima, T., Lavenu, F., Jankowiak, I., Smirnov, A., 1998. AERONET - a federated instrument network and data archive for aerosol characterization. Remote Sens. Environ. 66, 1–16.

Hsu, N.C., Jeong, M.J., Bettenhausen, C., Sayer, A.M., Hansell, R., Seftor, C.S., Huang, J., Tsay, S.C., 2013. Enhanced Deep Blue aerosol retrieval algorithm: the second

generation. J. Geophys. Res.: Atmosphere 118, 9296–9315.

Hsu, N.C., Tsay, S.C., King, M.D., Herman, J.R., 2004. Aerosol properties over bright-reflecting source regions. Ieee T Geosci Remote 42, 557–569.

Kikuchi, M., Murakami, H., Suzuki, K., Nagao, T.M., Higurashi, A., 2018. Improved hourly estimates of aerosol optical thickness using spatiotemporal variability derived from himawari-8 geostationary satellite. Ieee T Geosci Remote 56, 3442–3455.

Kim, Y.J., Kim, K.W., Kim, S.D., Lee, B.K., Han, J.S., 2006. Fine particulate matter characteristics and its impact on visibility impairment at two urban sites in Korea: seoul and Incheon. Atmos. Environ. 40 (Suppl. 2), 593–605.

Kodros, J.K., Scott, C.E., Farina, S.C., Lee, Y.H., L'Orange, C., Volckens, J., Pierce, J.R., 2015. Uncertainties in global aerosols and climate effects due to biofuel emissions. Atmos. Chem. Phys. 15, 8577–8596.

Kumabe, R., Kilshimoto, K., Sakurai, T., Nishimoto, Y., Hayashi, K., Inazawa, T., Kigawa, S., 1996. Meteorological Satellite Center: Technical Note.

Levy, R.C., Mattoo, S., Munchak, L.A., Remer, L.A., Sayer, A.M., Patadia, F., Hsu, N.C., 2013. The Collection 6 MODIS aerosol products over land and ocean. Atmospheric Measurement Techniques 6, 2989–3034.

Levy, R.C., Remer, L.A., Kleidman, R.G., Mattoo, S., Ichoku, C., Kahn, R., Eck, T.F., 2010. Global evaluation of the Collection 5 MODIS dark-target aerosol products over land. Atmos. Chem. Phys. 10, 10399–10420.

Li, J., Carlson, B.E., Lacis, A.A., 2013. Application of spectral analysis techniques in the intercomparison of aerosol data: 1. An EOF approach to analyze the spatial-temporal variability of aerosol optical depth using multiple remote sensing data sets. J. Geophys. Res. Atmos. 118, 8640–8648.

Li, S.S., Chen, L., Zheng, F., Han, D., Wang, Z., 2009. Design and application of haze optic thickness retrieval model for Beijing olympic games. In: Geoscience and Remote Sensing Symposium, 2009 IEEE International, IGARSS 2009, pp. II-507-II-510.

Li, Z.Q., Xu, H., Li, K.T., Li, D.H., Xie, Y.S., Li, L., Zhang, Y., Gu, X.F., Zhao, W., Tian, Q.J., Deng, R.R., Su, X.L., Huang, B., Qiao, Y.L., Cui, W.Y., Hu, Y., Gong, C.L., Wang, Y.Q., Wang, X.F., Wang, J.P., Du, W.B., Pan, Z.Q., Li, Z.Z., Bu, D., 2018. Comprehensive study of optical, physical, chemical, and radiative properties of total columnar atmospheric aerosols over China: an overview of sun–sky radiometer observation network (SONET) measurements. Bull. Am. Meteorol. Soc. 99, 739–755.

Long, X., Tie, X.X., Cao, J.J., Huang, R.J., Feng, T., Li, N., Zhao, S.Y., Tian, J., Li, G.H., Zhang, Q., 2016. Impact of crop field burning and mountains on heavy haze in the North China Plain: a case study. Atmos. Chem. Phys. 16, 9675–9691.

Malm, W.C., Sisler, J.F., Huffman, D., Eldred, R.A., Cahill, T.A., 1994. Spatial and seasonal trends in particle concentration and optical extinction in the United States. J. Geophys. Res.: Atmosphere 99, 1347–1370.

Martins, V.S., Lyapustin, A., de Carvalho, L.A.S., Barbosa, C.C.F., Novo, E.M.L.M., 2017. Validation of high-resolution MAIAC aerosol product over South America. J. Geophys. Res. Atmos. 122, 7537–7559.

Mhawish, A., Banerjee, T., Broday, D.M., Misra, A., Tripathi, S.N., 2017. Evaluation of MODIS Collection 6 aerosol retrieval algorithms over Indo-Gangetic Plain: implications of aerosols types and mass loading. Remote Sens. Environ. 201, 297–313.

Omar, A.H., Won, J.G., Winker, D.M., Yoon, S.C., Dubovik, O., McCormick, M.P., 2005. Development of global aerosol models using cluster analysis of Aerosol Robotic Network (AERONET) measurements. J. Geophys. Res. Atmos. 110, D10S14.

Onogi, K., Tsutsui, J., Koide, H., Sakamoto, M., Kobayashi, S., Hatsushika, H., Matsumoto, T., Yamazaki, N., Kamahori, H., Takahashi, K., Kadokura, S., Wada, K., Kato, K., Oyama, R., Ose, T., Mannoji, N., Taira, R., 2007. The JRA-25 reanalysis. Journal of the Meteorological Society of Japan. Ser. II 85, 369–432.

Sayer, A.M., Hsu, N.C., Bettenhausen, C., Jeong, M.J., 2013. Validation and uncertainty estimates for MODIS Collection 6 "Deep Blue" aerosol data. J. Geophys. Res. Atmos. 118, 7864–7872.

Sayer, A.M., Smirnov, A., Hsu, N.C., Holben, B.N., 2012. A pure marine aerosol model, for use in remote sensing applications. J. Geophys. Res. 117.

Tao, M., Chen, L., Wang, Z., Tao, J., Su, L., 2013. Satellite observation of abnormal yellow haze clouds over East China during summer agricultural burning season. Atmos. Environ. 79, 632–640.

Tao, M., Wang, Z., Tao, J., Chen, L., Wang, J., Hou, C., Wang, L., Xu, X., Zhu, H., 2017. How do aerosol properties affect the temporal variation of MODIS AOD bias in eastern China? Remote Sens-Basel 9, 800.

Tao, M.H., Chen, L.F., Wang, Z.F., Tao, J.H., Che, H.Z., Wang, X.H., Wang, Y., 2015. Comparison and evaluation of the MODIS Collection 6 aerosol data in China. J. Geophys. Res. Atmos. 120, 6992–7005.

Tie, X., Huang, R.-J., Dai, W., Cao, J., Long, X., Su, X., Zhao, S., Wang, Q., Li, G., 2016. Effect of heavy haze and aerosol pollution on rice and wheat productions in China. Sci. Rep. 6, 29612.

Wang, Z.F., Chen, L.F., Tao, J.H., Liu, Y., Hu, X.F., Tao, M.H., 2014. An empirical method of RH correction for satellite estimation of ground-level PM concentrations. Atmos. Environ. 95, 71–81.

Wei, J., Sun, L., Huang, B., Bilal, M., Zhang, Z., Wang, L., 2018. Verification, improvement and application of aerosol optical depths in China Part 1: inter-comparison of NPP-VIIRS and Aqua-MODIS. Atmos. Environ. 175, 221–233.

WHO, 2005. Air Quality Guidelines Global Update for Europe. World Health Organization, World Health Organization. WHO Regional Publications, Bonn, Germany.

Xie, D., Cheng, T., Wu, Y., Fu, H., Zhong, R., Yu, J., 2017. Polarized reflectances of urban areas: analysis and models. Remote Sens. Environ. 193, 29–37.

Yan, X., Li, Z., Luo, N., Shi, W., Zhao, W., Yang, X., Jin, J., 2018. A minimum albedo aerosol retrieval method for the new-generation geostationary meteorological satellite Himawari-8. Atmos. Res. 207, 14–27.

Yoshida, M., Kikuchi, M., Nagao, T.M., Murakami, H., Nomaki, T., Higurashi, A., 2018. Common retrieval of aerosol properties for imaging satellite sensors. J. Meteorol. Soc. Jpn. 96B, 193–209 (Ser. II advpub).

Yumimoto, K., Nagao, T.M., Kikuchi, M., Sekiyama, T.T., Murakami, H., Tanaka, T.Y., Ogi, A., Irie, H., Khatri, P., Okumura, H., Arai, K., Morino, I., Uchino, O., Maki, T., 2016. Aerosol data assimilation using data from Himawari-8, a next-generation geostationary meteorological satellite. Geophys. Res. Lett. 43, 5886–5894.

Zhang, Q., Jiang, X., Tong, D., Davis, S.J., Zhao, H., Geng, G., Feng, T., Zheng, B., Lu, Z., Streets, D.G., Ni, R., Brauer, M., van Donkelaar, A., Martin, R.V., Huo, H., Liu, Z., Pan, D., Kan, H., Yan, Y., Lin, J., He, K., Guan, D., 2017a. Transboundary health impacts of transported global air pollution and international trade. Nature 543, 705–709.

Zhang, Z., Wu, W., Wei, J., Song, Y., Yan, X., Zhu, L., Wang, Q., 2017b. Aerosol optical depth retrieval from visibility in China during 1973–2014. Atmos. Environ. 171, 38–48.

Zhang, Z.Y., Wong, M.S., 2017. A simplified method for retrieving aerosol optical thickness using visibility data between 1980 and 2014, a case study in China. Ieee J-Stars 10, 4409–4416.

Zhang, Z.Y., Wong, M.S., Campbell, J.R., 2018. Conceptualizing How Severe Haze Events Are Impacting Long-term Satellite-based Trend Studies of Aerosol Optical Thickness over Asia. Springer, Cham.

Zhang, Z.Y., Wong, M.S., Lee, K.H., 2016a. Evaluation of the representativeness of ground-based visibility for analysing the spatial and temporal variability of aerosol optical thickness in China. Atmos. Environ. 147, 31–45.

Zhang, Z.Y., Wong, M.S., Nichol, J., 2016b. Global trends of aerosol optical thickness using the ensemble empirical mode decomposition method. Int. J. Climatol. 36, 4358–4372.